Dynamics Study of the OH + O$_2$ Branching Atmospheric Reaction. 3. Dissociation in Collisions of Vibrationally Excited Reactants

**P. J. S. B. Caridade, M. Betancourt,[†] J. D. Garrido,[†] and A. J. C. Varandas*,[‡]**

*Departamento de Química, Universidade de Coimbra, P-3049 Coimbra Codex, Portugal*

We discuss the dissociation of the OH radical in the title molecular collisions when both species are vibrationally excited. An analysis of the O$_2$ dissociation is also reported. All calculations employed the quasiclassical trajectory method and a realistic double many-body expansion (DMBE) potential energy surface for ground-state HO$_3$. The results are compared with those referring to formation of HO$_2$ and O$_3$ under similar conditions. Possible implications on atmospheric models for ozone production are tentatively assessed.

1. Introduction

Production of vibrational−rotational excited OH radicals and O$_2$ molecules, heretofore denoted as OH(v') and O$_2$(v''), has been observed in several atmospheric reactions; for a recent review on theoretical work, see ref 1. For example, the reaction

$$H + O_3 \rightarrow OH(X^2\Pi, v') + O_2 \qquad (1)$$
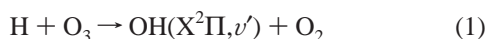
leads to OH in vibrationally excited states with quantum numbers up to $v' = 9$.[2−13] In turn, photodissociation of ozone within the Hartley band yields vibrationally excited molecular oxygen with a distribution peaking in the vicinity of $v'' = 14$ and $v'' = 27$[14] according to the reaction

$$O_3 + h\nu(\lambda < 243 \text{ nm}) \rightarrow O_2(X^3\Sigma_g^-, v'') + O(^3P) \qquad (2)$$
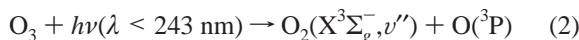
Recently, another bimodal distribution has been observed in the photodissociation of ozone at 266 nm with peaks near $v'' = 9$ and $v'' = 5$.[15] An additional source of vibrationally excited oxygen molecules in the stratosphere is the reaction[16]

$$O + HO_2 \rightarrow O_2(X^3\Sigma_g^-, v'') + OH \qquad (3)$$
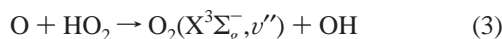
with O$_2$ populating vibrationally excited levels up to $v'' = 13$. Similarly, the reaction

$$O + O_3 \rightarrow O_2(X^3\Sigma_g^-, v'') + O_2 \qquad (4)$$
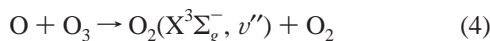
is known to yield vibrationally excited molecular oxygen with quantum numbers $v'' \leq 14$.[14,17] The existence in the stratosphere of such vibrationally hot species under conditions of nonlocal thermodynamic equilibrium (non-LTE) or "local thermodynamic disequilibrium" allows the occurrence of endoenergetic reactions which would not be viable otherwise.[1,18] In a series of papers[19−21] (hereafter referred to as I−III), we have studied the role of the internal energy of the reactants in the branching

reaction

$$OH(v', j') + O_2(v'', j'') \rightarrow HO_2 + O \qquad (5)$$

$$\rightarrow O_3 + H \qquad (6)$$
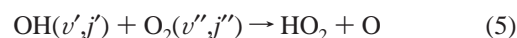
However, the study of reactants dissociation under such conditions remains unanswered. In relation to ozone formation it is an interesting problem because dissociation of both reactants lead to formation of atomic oxygen, which will then form ozone by the three-body recombination reaction

$$O(^3P) + O_2 + M \rightarrow O_3 + M \qquad (7)$$
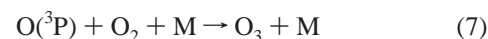
The OH radical has attracted much attention in recent years, in particular its photodissociation.[22,23] However, to our knowledge, no single study of OH collisional dissociation has been reported. Although quantum models have been developed to describe the dissociation process,[24] the use of computational procedures based on the quasiclassical trajectory (QCT) approach makes such a study easier and also general for collisions involving polyatomic systems (for example, a QCT study of dissociation in H$_2$ + H$_2$ collisions has been recently reported.[25] A major goal of the present work is therefore to report a detailed QCT study of the reaction

$$OH(v', j') + O_2(v'', j'') \rightarrow O_2 + H + O \qquad (8)$$
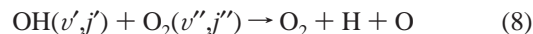
by considering various combinations of vibrational and rotational excitations. For this, as in papers I[19] and II,[20] we employ a realistic single valued DMBE potential energy surface[26] for the electronic ground state of HO$_3$. This function will be denoted from now on as DMBE I, since an improved potential energy surface (DMBE II) has recently been reported[27]

$$H + O_3 \rightarrow OH + O_2 \qquad (9)$$

for this system based on accurate QCISD/CBS (quadratic configuration interaction including single and double electron excitations extrapolated to the complete basis set limit) calculations. This DMBE II potential energy surface has already been employed in paper III,[21] although we use here DMBE I for consistency with previous studies in papers I[19] and II[20] (see also refs 16, 26, 28−30).

† Permanent address: Departamento de Física General y Matemática, Instituto Superior de Ciencias y Tecnología Nucleares, 6163 La Habana, Cuba.
‡ E-mail: varandas@qtvs1.qui.uc.pt.

TABLE 1: Summary of the Trajectory Calculations for OH(v',j'=1) + O$_2$(v'',j''=1) → H + O + O$_2$

v'	v''	$E_{vib/rot}$, kcal mol^{-1}	E_{tr}, kcal mol^{-1}	b_{max}, Å	$\sigma^{O-H} \pm \Delta\sigma^{O-H}$, Å^2
6	13	111.10	0.5	4.8	1.09 ± 0.20
			1.0	4.2	0.64 ± 0.14
			2.5	3.9	0.62 ± 0.12
			5.0	3.4	0.46 ± 0.09
			10.0	3.0	0.81 ± 0.11
6	16	121.62	0.5	6.0	5.32 ± 0.53
			1.0	5.1	4.13 ± 0.40
			2.5	4.1	3.01 ± 0.27
			5.0	3.9	2.46 ± 0.24
			10.0	3.7	2.56 ± 0.23
3	27	128.45	0.5	6.0	9.00 ± 0.71
			1.0	5.8	7.34 ± 0.60
			2.5	5.4	4.85 ± 0.46
			5.0	4.7	3.68 ± 0.35
			10.0	4.0	3.00 ± 0.27
9	13	131.48	0.5	6.0	9.50 ± 0.70
			1.0	5.3	6.91 ± 0.52
			2.5	4.4	5.00 ± 0.37
			5.0	4.0	4.47 ± 0.32
			10.0	4.2	3.61 ± 0.30
9	16	142.00	0.5	6.1	14.79 ± 0.87
			1.0	5.6	11.43 ± 0.70
			2.5	5.4	8.20 ± 0.58
			5.0	4.8	6.48 ± 0.46
			10.0	4.5	6.23 ± 0.42
6	27	153.48	0.5	6.3	16.90 ± 0.96
			1.0	6.0	14.50 ± 0.84
			2.5	5.6	11.10 ± 0.69
			5.0	5.2	9.51 ± 0.60
			10.0	4.8	8.03 ± 0.47
9	27	173.85	0.5	6.2	19.80 ± 1.00
			1.0	6.0	16.96 ± 0.90
			2.5	5.7	14.85 ± 0.80
			5.0	5.4	12.18 ± 0.69
			10.0	5.2	12.02 ± 0.66

TABLE 2: Summary of the Trajectory Calculations for OH(v' j') + O$_2$(v''=16,j'') → H + O + O$_2$

v'	j'	j''	$E_{vib/rot}$, kcal mol^{-1}	E_{tr}, kcal mol^{-1}	b_{max}, Å	$\sigma^{O-H} \pm \Delta\sigma^{O-H}$, Å^2
9	10	1	145.63	5.0	4.3	6.36 ± 0.41
				2.5	4.7	8.22 ± 0.50
	1	9	142.29	5.0	4.7	6.77 ± 0.46
				2.5	5.3	6.71 ± 0.52
6	10	1	125.99	5.0	3.8	3.13 ± 0.26
				2.5	4.0	2.81 ± 0.26
	1	9	121.91	5.0	4.0	2.34 ± 0.24
				2.5	4.3	2.44 ± 0.26

The paper is organized as follows. Section 2 provides a brief survey of the computational method. The results are presented and discussed in section 3, while the major conclusions are in section 4.

2. Computational Details

Following previous work, the QCT method as implemented in extensively adapted versions of the MERCURY/VENUS96[31] codes has been used for the present study. Calculations have been carried out for diatom−diatom translations energies over the range $0.5 \leq E_{tr}/\text{kcal mol}^{-1} \leq 10$, as summarized in Tables 1 and Table 2. Thus, we focus the computational effort in the range of small and middle translational energies, which are likely to be of major interest in modeling atmospheric chemistry. The optimum step size for numerical integration of the equations of motion was obtained as in previous papers, and found to be 10^{-16} s (this warrants energy conservation up to 2 parts in 10^5). The initial diatomic-diatomic separation has been fixed at 8 Å to make the interaction essentially negligible. For each set of initial conditions, the maximum value of the impact parameter (b_{max}) which leads to reaction has been determined according
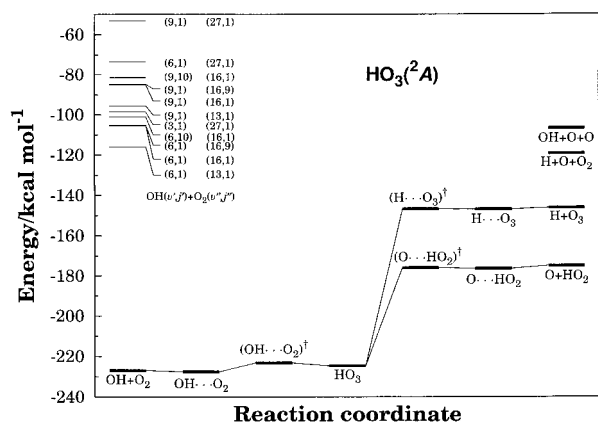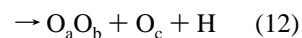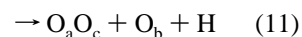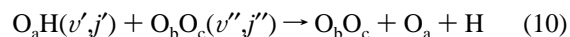

Figure 1. Schematic diagram showing the energetics of the title reaction according to the HO$_3$ DMBE I potential energy surface. For a comparison with DMBE II, see ref 21.

to the usual procedure, leading to an accuracy of about ±0.1 Å; the calculated values are reported in Tables 1 and 2. Batches of 2000 trajectories have then been carried out for each translational energy and vibrational−rotational combination making a total of 8.6×10^4 trajectories. The energetics of the involved processes is best seen in the diagram of Figure 1, which indicates by the line segments on the reactants side the various vibrational−rotational combinations according to the HO$_3$ DMBE I potential energy surface[26] employed in this work. As seen, they are all quite above the energy of the transition state for reaction. This implies that the QCT technique is ideally suited for the present study as the number of accessible states is so large that quantum results are nearly impossible at such high energies.

3. Results and Discussion

Tables 1 and 2 summarize the trajectory calculations carried out in the present work for the title dissociative reaction. For the calculations we have considered three distinct channels leading to OH dissociation

$$O_aH(v',j') + O_bO_c(v'',j'') \rightarrow O_bO_c + O_a + H \quad (10)$$

$$\rightarrow O_aO_c + O_b + H \quad (11)$$

$$\rightarrow O_aO_b + O_c + H \quad (12)$$

where the indices a, b, and c label the three oxygen atoms. In the case of indistinguishable atoms, the reactions in eqs 11 and 12 have similar probabilities of occurrence with the percentage of reaction in eq 10 increasing with internal energy of OH. Thus, we will consider only their sum in the following discussion. For total internal energies close to 111 kcal mol^{-1}, which corresponds to the combination OH(v'=6, j' = 1) + O$_2$-(v''=13,j''=1), the cross section for dissociation is small. Thus, we may consider this combination as the bottom limit for an effective dissociation process (for the same internal and translational energies, one gets cross sections which are an order of magnitude smaller than those for the process yielding HO$_2$). Clearly, the dissociation channel gets closed for energy combinations below the threshold given by the corresponding endoergicity.

Parts a and b of Figure 2 show typical opacity functions (reaction probability vs impact parameter) for dissociation of OH in barrier-type (which is observed at high translational energies) and capture-type (small translational energies) regimes.
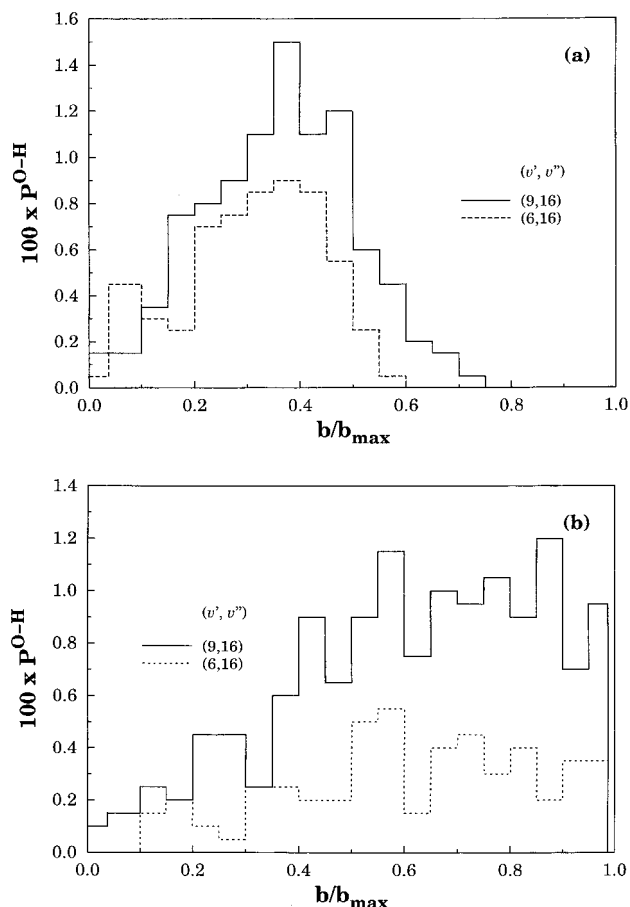
PH + O₂ Branching Atmospheric Reaction

J. Phys. Chem. A, Vol. 105, No. 31, 2001 **7437**

Figure 2. Opacity function for OH dissociation: (a) barrier-type mechanism for $E_{tr} = 10$ kcal mol^{-1}; (b) capture-type mechanism for $E_{tr} = 0.5$ kcal mol^{-1}.

Note that the abscissae in these plots are b/b_{max}, with b_{max} being the largest impact parameter calculated in the present work (6.3 Å). Thus, for high translational energies (part a), the opacity function shows a bell shape (common for reactions with a threshold energy), while for low translational energies (part b), it increases with impact parameter showing the effect of long-ranges forces. As in previous papers,[19–21] we encounter both mechanisms in the collisional processes described in the present work.

3.1. Reactive Cross Sections. For a given value of the translational energy, the specific reactive cross section for OH dissociation and associated 68% uncertainty assume the form given in eqs 10 and 11 of ref 20 with $x = $ O–H. We now examine the shape of the excitation functions (cross section vs translational energy) for the dissociation of OH which are shown in Figure 3 together with the associated error bars. For low translational energies, the capture-type regime is seen to dominate over the whole range of internal energies considered in the present work leading to the well established (refs 32, 33, and references therein) decreasing dependence of the reactive cross section with E_{tr}. On the other hand, for high translational energies, one observes a dependence $\sigma_{v'j',v''j''}^{O-H}$ vs E_{tr} where the derivative changes gradually from negative to slightly positive with increasing internal energy. Such a behavior means that, for high translational and internal energies, the contribution of the barrier-type regime becomes significant. Further details concerning this type of mechanism can be found elsewhere.[19–21]

As noted in papers I[19] and II[20], for a given vibrational–rotational state of one of the reactant molecules, the effect of rotational excitation in the other partner is essentially an
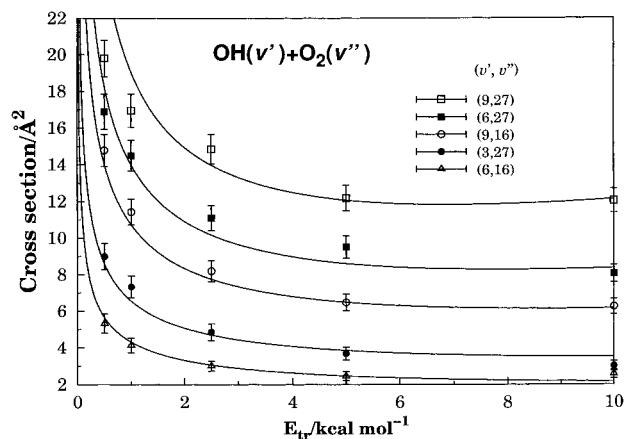

Figure 3. Reactive cross section σ^{O-H} as a function of the translational energy. Also indicated are the *68% error bars*. In all cases $j' = j'' = 1$.

energetic one, being larger for OH due to the higher value of the rotational quanta. We find such an effect to be extensive (within error bars) to the collisional dissociation of OH. However, it is not as significant as in previous work[19,20] due to the higher levels of internal energy required to promote dissociation. Table 2 presents the results obtained for several combinations having similar total internal energies and rotational quantum numbers $j' = 10$ and $j'' = 9$. These correspond to the optimal populations,[16,28] as given by the maximum of the associated Maxwell–Boltzmann rotational distributions (i.e., we assume a thermalized distribution of rotational energies). It is seen that the calculated cross sections are roughly dictated by the amount of total energy involved. This suggests that we may keep the form employed elsewhere[19–21] to describe the dependence of the dissociation cross section on translational energy.

Following previous work,[19–21] we then write

$$\sigma^{O-H}(E_{OH}, E_{O_2}, E_{tr}) = \frac{f(E_{OH}, E_{O_2})}{E_{tr}^n} +$$
$$g(E_{OH}, E_{O_2})E_{tr}^p \exp(-mE_{tr}) \quad (13)$$

where all symbols have their usual meaning. However, the auxiliary functions are now defined by

$$f(E_{OH}, E_{O_2}) = a_0 + a_1 x + a_2 x^2 \quad (14)$$

$$g(E_{OH}, E_{O_2}) = b_0 + b_1 x + b_2 x^2 \quad (15)$$

where

$$x = \frac{E_{OH} + E_{O_2} - E_{th}}{E_{th}} \quad (16)$$

and the threshold energy is $E_{th} = 111$ kcal mol^{-1}. The numerical values of parameters m, n, and p have been constrained to assume the same value for all reactive processes, and fixed by a trial and error procedure. The remaining coefficients in eqs 14 and 15 have been determined from a global least-squares fitting procedure; the optimum numerical values of all fitting parameters are reported in Table 3. The resulting fitted functions are shown together with the calculated points in Figure 3. It is seen that the model fits well the calculated data. Note that in papers I[19] and II[20] the value of n was fixed at $n = 1/2$, which stemmed from the assumption that the dependence of the cross

TABLE 3: Numerical Values^a of Coefficients in Equation 13

m	0.02	n	0.4	p	1.2
a_0	0.652 116	a	39.041 9	a_2	−12.537 5
b_0	−0.015 531 6	b_1	0.507 74	b_2	0.287 34

^{a} The units are such that when the energy is given in kcal mol^{-1} the cross section are Å^2.

section on E_{tr} was essentially determined by the long-range dipole−quadrupole electrostatic interaction. Despite this being the leading long-range interaction between OH and O$_2$, the potential energy surface contains also higher-order interaction contributions, and hence we have recommended[21] to treat n as an effective parameter to improve the quality of the least-squares fit. Note also that the representation depends essentially on the magnitude of the internal energy, but not so much on the model employed to express the dependence of the latter on the quantum numbers.

From the reactive cross section and assuming a Maxwell−Boltzmann distribution over the translational energy (E_{tr}), the specific thermal rate coefficient is obtained as

$$k_{v'j',v''j''}^{O-H}(T) = g_e(T)\left(\frac{2}{k_BT}\right)^{3/2}\left(\frac{1}{\pi\mu}\right)^{1/2}\int E_{tr}\sigma_{v'j',v''j''}^{O-H}\exp\left(-\frac{E_{tr}}{k_BT}\right)dE_{tr} \tag{17}$$

where k_B is the Boltzmann constant, μ is the reduced mass of the colliding diatomic particles, and T is the temperature. In turn, $g_e(T) = \frac{1}{3}[1 + \exp(-205/T)]^{-1}$ is the appropriate electronic degeneracy factor, which corresponds to the ratio of the electronic partition functions; note that the spin−orbit excited level of OH ($^2\Pi_{1/2}$) lies 205 K above that of ground state ($^2\Pi_{3/2}$)[34] (see also ref 35, and references therein). One then obtains

$$k^{O-H}(E_{OH},E_{O_2},T) = g_e(T)\left(\frac{8}{\pi\mu}\right)^{1/2}(k_BT)^{1/2-n} \times$$
$$\left[\Gamma(2-n)f(E_{OH},E_{O_2}) + \Gamma(p+2)g(E_{OH},E_{O_2})\frac{(k_BT)^{p+n}}{(1+mk_BT)^{2+p}}\right] \tag{18}$$

where $\Gamma(\cdots)$ is the gamma function. In papers I[19] and II[20], with $n = \frac{1}{2}$, the temperature dependence in eq 18 was essentially determined by the electronic degeneracy factor $g_e(T)$, having now the factor $(k_BT)^{1/2-n}$ a marked influence.

For very high temperatures ($mk_BT \gg 1$) and values of n such that $\frac{1}{2} - n > 0$, a simple algebraic analysis shows that eq 18 can be approximated by

$$k^{O-H}(E_{OH},E_{O_2},T) = g_e(T)\left(\frac{8}{\pi\mu}\right)^{1/2}(k_BT)^{1/2-n} \times$$
$$\left[\Gamma(2-n)f(E_{OH},E_{O_2}) + \Gamma(p+2)g(E_{OH},E_{O_2})\frac{(1/m)^{p+n}}{(mk_BT)^{2-n}}\right] \tag{19}$$

On the other hand, for low temperatures ($mk_BT \ll 1$), one obtains

$$k^{O-H}(E_{OH},E_{O_2},T) = g_e(T)\left(\frac{8}{\pi\mu}\right)^{1/2}(k_BT)^{1/2-n} \times$$
$$\left[\Gamma(2-n)f(E_{OH},E_{O_2}) + \Gamma(p+2)g(E_{OH},E_{O_2})\frac{(mk_BT)^{p+n}}{(m)^{n+p}}\right] \tag{20}$$
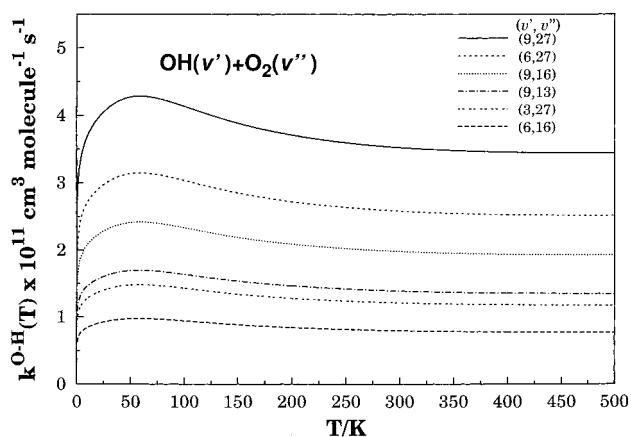

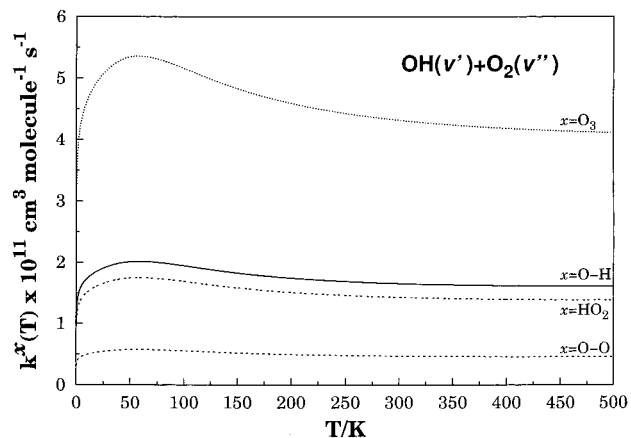**Figure 4.** Specific rate coefficients of the title reaction for several internal energies.

Figure 5. Average thermal rate coefficients for the title reaction. Also shown is the thermal rate coefficient for formation of O$_3$ and HO$_2$, and dissociation of O$_2$.

which should be valid for most temperature regimes of practical interest, including those considered in the present work. In both limits, eqs 19 and 20, the factor $(k_BT)^{1/2-n}$ essentially determines the functional dependence on temperature. Equation 18 shows a maximum at low temperatures (T_{max}), which can be calculated from the numerical solution of the equation $1/2 - n = \xi[\exp(-\xi)/1 + \exp(-\xi)]$, where $\xi = 205/T$. This leads to $T_{max} \sim 58$ K. Note that the shape of the specific thermal rate coefficients for formation of HO$_2$ and O$_3$, and dissociation of OH, are all very similar; the only difference is on their magnitudes. Figure 4 shows the curves in eq 18 for several values of the internal energy. For the reasons given above, the details concerning the rate of increase with T for ultralow temperatures should be seen with caution in Figure 4 (and the following). In fact, quantum tunneling effects may also be not negligible at such ultralow-temperature regimes.

In Figure 5 we present, for a given vibrational distribution, the calculated thermal rate constant for OH dissociation. It assumes the form

$$k^{O-H}(T) = \frac{\displaystyle\sum_{v'=v'_0}\sum_{v''=v''_0} w_{v'}w_{v''}k^{O-H}(E_{OH}(v',j'=10), E_{O_2}(v'',j''=1))}{\displaystyle\sum_{v'=0}\sum_{v'=0} w_{v'}w_{v''}} \tag{21}$$

where $v'_0 = 4$ and $v''_0 = 0$. The populations $w_{v''}$ for the

TABLE 4: Summary of the Trajectory Calculations for OH(v',j'=1) + O$_2$(v'',j''=1) → OH + O + O

v'	v''	$E_{vib/rot}$, kcal mol^{-1}	E_{tr}, kcal mol^{-1}	b_{max}, Å	$\sigma^{O-O} \pm \Delta\sigma^{O-O}$, Å^2
9	13	131.48	0.5	6.0	0.50 ± 0.17
			1.0	4.9	0.43 ± 0.12
			2.5	4.4	0.39 ± 0.11
			5.0	4.0	0.45 ± 0.10
			10.0	4.2	0.64 ± 0.13
9	16	2.00	0.5	6.1	2.57 ± 0.38
			1.0	5.6	2.22 ± 0.33
			2.5	5.4	1.88 ± 0.29
			5.0	4.8	1.41 ± 0.22
			10.0	4.5	1.11 ± 0.19
6	27	153.48	0.5	6.3	7.86 ± 0.67
			1.0	6.0	6.39 ± 0.58
			2.5	5.6	4.78 ± 0.47
			5.0	5.2	4.08 ± 0.40
			10.0	4.6	3.89 ± 0.35
9	27	173.85	0.5	6.2	12.14 ± 0.81
			1.0	6.0	9.90 ± 0.71
			2.5	5.7	7.55 ± 0.60
			5.0	5.4	6.69 ± 0.53
			10.0	5.2	4.80 ± 0.44

vibrational state v'' of oxygen have been assumed to be those obtained in the 226 nm photolysis of ozone,[14] while the populations $w_{v'}$ for the state v' of the OH radical are taken from ref 8. Of course, many other factors (including a scanning over the complete range of ozone-photolysis wavelengths) should be taken in consideration when fully assessing the implications of the present results in atmospheric chemistry. This is out of the scope of the present work, and hence the results given here should be taken as illustrative ones. As Figure 5 shows, the vibrationally averaged thermal rate coefficient for OH dissociation slightly increases for very low temperatures showing a maximum at the temperature mentioned above. After the maximum it decreases with temperature from about 2.01×10^{-11} cm^3 molecule^{-1} s^{-1} at $T \sim 58$ K to about 1.60×10^{-11} cm^3 molecule^{-1} s^{-1} at $T \sim 500$ K. Nevertheless, considering the peaks reported for the photodissociation of O$_3$ at 266 nm,[15] we can expect eq 21 to underestimate the real value of $k^{O-H}(T)$. Also shown for completeness in Figure 5 are the calculated vibrationally averaged thermal rate coefficients for formation of O$_3$ and HO$_2$, which have been calculated in a similar way but using an optimized n value. The thermal rate coefficients for O$_3$ formation are seen to be a factor of about 2.5 larger than the corresponding rates for dissociation of OH. In turn, those for HO$_2$ formation are slightly smaller than for dissociation of OH. For completeness, we also give for comparison in Figure 5 the average thermal rate coefficient for O$_2$ dissociation. As seen, its value as a function of temperature is about 3 times smaller than $k^{O-H}(T)$. Although the cross sections calculated for O$_2$ dissociation (see Table 4) have not employed values of the impact parameter specifically optimized for this process, test calculations for a few sets of initial conditions have shown that the results given here should also be reliable.

The consideration in atmospheric models of the reactions in eqs 1–4, together with an effective mechanism for relaxation of the vibrational energy, lead to depletion of atmospheric ozone. However, as shown in paper II[20] of this series and also in this paper, the rates for the reactions 5, 6, and 8 have magnitudes of 10^{-10}–10^{-11} cm^3 molecule^{-1} s^{-1}, which overpass the reported vibrational relaxation rate constant for the processes O$_2$(v'') + O$_2$,[36–39] OH(v') + O$_2$,[12,13] and OH(v') + O$_3$.[40,41] This is best seen from Table 5, which compares such data with the rate constant values calculated in the present work. Moreover, by considering that the atomic oxygen produced in eq 5 and eq

TABLE 5: Theoretical and Experimental Vibrational Relaxation Rate Constants (in cm^3 molecule^{-1} s^{-1}) Involving OH and O$_2$ Species^a

O$_2$(v''=27) + O$_2$(v''=0) → O$_2$(v'') + O$_2$(v'')^b	
v'' = 27	0.5(−12)
OH(v') + O$_2$ → OH(v'−1) + O$_2$^{c}	
v' = 1	1.3 ± 0.4(−13)
v' = 2	2.7 ± 0.8(−13)
v' = 3	5.2 ± 1.5(−13)
v' = 4	8.8 ± 3.0(−13)
v' = 5	17 ± 7(−13)
v' = 6	30 ± 15(−13)
v' = 7^d	7 ± 2(−12)
OH(v') + O$_3$ → OH(v'=0) + O$_3$^{e}	
v' = 1	1.0(−12)

^{a} The powers of 10 by which the numbers should be multiplied are given in brackets. For other results, see the original papers. ^{b} Reference 37, for $T = 460$ K. ^{c} Reference 12. ^{d} Reference 42. ^{e} Reference 40.

8 (together with that produced in O$_2$ dissociation) can generate ozone through the three-body recombination reaction in eq 7, one is led to expect a significant influence of the reactions studied in the present work in kinetic models of stratospheric ozone. Of course, a quantitative assessment can only be made through atmospheric modeling simulations which include (or do not include) such reactions. Their importance can be further strengthened bearing in mind that the improved HO$_3$ DMBE II potential energy surface leads to a prediction[21] about 50% larger for direct production of ozone through the reaction in eq 6.

To conclude, we have calculated the total vibrationally average thermal rate coefficients for the reactions in eqs 5–8, and dissociation of O$_2$, by using

$$k^{total}(T) = \frac{\displaystyle\sum_{v'=v'_0}\sum_{v''=v''_0} w_{v'}w_{v''}N_i^{odd}\sum_i k^i(E_{OH}(v',j'{=}10), E_{O_2}(v'',j''{=}1))}{\displaystyle\sum_{v'=0}\sum_{v''=0} w_{v'}w_{v''}}$$

(22)

where i stands for each of the four above-mentioned processes, and N_i^{odd} stands for the number of product "odd-oxygen" species (i.e., O and/or O$_3$); v'_0 and v''_0 assume the values indicated above. Thus, it represents the total reactive rate constant leading to ozone formation. The value of this total rate for a typical stratospheric temperature of $T = 150$ K is $k^{total} = 9.27 \times 10^{-11}$ cm^3 molecule^{-1} s^{-1}. As seen, it is about an order of magnitude larger than the corresponding vibrational relaxation rates reported in the literature, as well as the rate suggested in ref 17 for the process O$_2$(v',j') + O$_2$(v'',j'') → O$_3$ + O, $k \sim 6.5 \times 10^{-12}$ cm^3 molecule^{-1} s^{-1}.

Conclusions

We have carried out a QCT study of molecular dissociation in the OH(v', j') + O$_2$(v'',j'') reaction for several combinations of rotational and vibrational quantum numbers. The results have shown that OH dissociation and ozone formation via collisions of vibrationally excited OH and O$_2$ molecules are comparable over the same range of collisional energies. In particular, the cross section for O$_3$ formation has been found to be nearly twice as large as that of OH dissociation for the initial conditions studied in the present work (for formation of HO$_2$, see paper II[20]). Finally, we have pointed out that the title dissociative processes provide extra sources of ozone through a three-body

7440 *J. Phys. Chem. A, Vol. 105, No. 31, 2001*

Caridade et al.

recombination reaction with molecular oxygen. Thus, they should not be overlooked when discussing the so-called 'ozone deficit' problem.

References and Notes

(1) Varandas, A. J. C. *Int. Rev. Phys. Chem.* **2000**, *19*, 199.
(2) Polanyi, J. C.; Sloan, J. J. *Int. J. Chem. Kinet. Symp.* **1975**, *1*, 51.
(3) Greenblatt, G. D.; Wiesenfeld, J. R. *J. Geophys. Res.* **1982**, *87*, 11145.
(4) Finlayson-Pitts, B. J.; Kleindienst, T. E.; Ezell, M. J.; Toohey, D. W. *J. Chem. Phys.* **1981**, *74*, 4533.
(5) Washida, N.; Akimoto, H.; Okuda, M. *J. Chem. Phys.* **1980**, *72*, 5781.
(6) Howard, C. J.; Finlayson, B. J. *J. Chem. Phys.* **1980**, *72*, 3842.
(7) Force, A. P.; Wiesenfeld, J. R. *J. Chem. Phys.* **1981**, *74*, 1718.
(8) Ohoyama, H.; Kasai, T.; Yoshimura, Y.; Kuwata, H. *Chem. Phys. Lett.* **1985**, *118*, 263.
(9) Zhurt, C.; Zülicke, L.; Umansky, S. Y. *Chem. Phys.* **1986**, *105*, 15.
(10) Zhurt, C.; Zülicke, L. *Chem. Phys. Lett.* **1984**, *111*, 408.
(11) Shalashilin, D. V.; Umanskii, S. Y.; Gershenzon, Y. M. *Chem. Phys.* **1992**, *168*, 315.
(12) Dodd, J. A.; Lipson, S. J.; Blumberg, W. A. M. *J. Chem. Phys.* **1991**, *95*, 5752.
(13) Shalashilin, D. V.; Michtchenko, A. V.; Umanskii, S.; Gershenzo, Y. M. *J. Phys. Chem.* **1995**, *99*, 11627.
(14) Miller, R. L.; Suits, A. G.; Houston, P. L.; Toumi, R.; Mack, J. A.; Wodtke, A. M. *Science* **1994**, *265*, 1831.
(15) Geiser, J.; Dylewski, S. M.; Mueller, J. A.; Willson, R. J.; Toumi, R.; Houston, P. L. *J. Chem. Phys.* **2000**, *112*, 1279.
(16) Wang, W.; González-Jonte, R.; Varandas, A. J. C. *J. Phys. Chem. A* **1998**, *102*, 6935.
(17) Varandas, A. J. C.; Wang, W. *Chem. Phys.* **1997**, *215*, 167.
(18) Yang, X.; Price, J. M.; Mack, J. A.; Morgan, C. G.; Rogaski, C. A.; McGuire, D.; Kim, E. H.; Wodtke, A. M. *J. Phys. Chem.* **1993**, *93*, 3944.
(19) Garrido, J. D.; Caridade, P. J. S. B.; Varandas, A. J. C. *J. Phys. Chem. A* **1999**, *103*, 4815.
(20) Caridade, P. J. S. B.; Zhang, L.; Garrido, J. D.; Varandas, A. J. C. *J. Phys. Chem. A* **2001**, *105*, 4395.
(21) Varandas, A. J. C.; Caridade, P. J. S. B. *Chem. Phys. Lett.* **2001**, *339*, 1.
(22) Lee, S. *J. Chem. Phys.* **1999**, *111*, 6407.
(23) Parlant, G.; Yarkony, D. *J. Chem. Phys.* **1999**, *110*, 363.
(24) Hernández, M. I.; Clary, D. C. *J. Chem. Phys.* **1996**, *104*, 8413.
(25) Ceballos, A.; Garcia, E.; Rodríguez, A.; Laganá, A. *Chem. Phys. Lett.* **1999**, *305*, 276.
(26) Varandas, A. J. C.; Yu, H. G. *Mol. Phys.* **1997**, *91*, 301.
(27) Yu, H. G.; Varandas, A. J. C. *Chem. Phys. Lett.* **2001**, *334*, 173.
(28) Yu, H. G.; Varandas, A. J. C. *J. Chem. Soc., Faraday Trans.* **1997**, *93*, 2651.
(29) Szichman, H.; Baer, M.; Varandas, A. J. C. *J. Phys. Chem. A* **1997**, *101*, 8817.
(30) Varandas, A. J. C.; Szichman, H. *Chem. Phys. Lett.* **1998**, *295*, 113.
(31) Hase, W. L. MERCURY: a general Monte Carlo classical trajectory computer program, *QCPE* No. 453. For an updated version of this code, see: VENUS96: Hase, W. L.; Duchovic, R. J.; Hu, X.; Komornik, A.; Lim, K. F.; Lu, D.-H.; Peslherbe, G. H.; Swamy, K. N.; van de Linde, S. R.; Varandas, A. J. C.; Wang, H.; Wolf, R. J. *QCPE Bull* **1996**, *16*, 43.
(32) Smith, I. W. *Kinetics and Dynamics of Elementary Gas Reactions*; Butterworth: Boston, 1980.
(33) Levine, R. D.; Bernstein, R. B. *Molecular Reaction Dynamics and Chemical Reactivity*; Oxford University Press: New York, 1987.
(34) Clary, D. C.; Werner, H.-J. *Chem. Phys. Lett.* **1984**, *112*, 346.
(35) Varandas, A. J. C. *J. Chem. Phys.* **1993**, *99*, 1076.
(36) Billing, G. D.; Kolesnick, R. E. *Chem. Phys. Lett.* **1992**, *200*, 382.
(37) Balakrishnan, N.; Dalgarno, A.; Billing, G. D. *Chem. Phys. Lett.* **1998**, *288*, 657.
(38) Rogaski, C. A.; Mack, J. A.; Wodtke, A. M. *Faraday Discuss. Atmos. Chem.* **1995**, *100*, 229.
(39) Jongma, R. T.; Wodtke, A. M. *J. Chem. Phys.* **1999**, *111*, 10957.
(40) Teitelbaum, H.; Aker, P.; Sloan, J. *J. Chem. Phys.* **1988**, *119*, 79.
(41) Varandas, A. J. C.; Zhang, L. *Chem. Phys. Lett.* **2001**. In press.
(42) Knutsen, K.; Dyer, M. J.; Copeland, R. A. *J. Chem. Phys.* **1996**, *104*, 5798.